Frequency Domain Numerical Dispersion Mitigation Network

Kirill Gadylshin[1(✉)], Vadim Lisitsa[2], Kseniia Gadylshina[2], and Dmitry Vishnevsky[2]

[1] LLC RN-BashNIPIneft, 3/1 Behtereva st., Ufa 450103, Russia
gadylshin@gmail.com
[2] Institute of Petroleum Geology and Geophysics SB RAS, 3 Koptug ave., Novosibirsk 630090, Russia

Abstract. This study proposes using an NDM-net in the frequency domain to mitigate numerical dispersion in seismic data, a major problem in the petroleum industry. Frequency-domain processing has several advantages over time-domain processing, including more efficient extraction of information from large datasets, noise removal, and correction for amplitude and phase distortions. The proposed approach can significantly improve the exploration and characterization of hydrocarbon reservoirs, with Full Waveform Inversion (FWI) being a prominent example. To evaluate the proposed method, we applied it to a realistic synthetic BP numerical example, resulting in an average reduction of numerical dispersion by a factor of three and an order-of-magnitude increase in calculation performance. The proposed approach enables us to process the entire seismogram simultaneously, in contrast to the time-domain NDM-net implementation and thus can be applied to 3D seismic modeling. Overall, the use of NDM-net in the frequency domain can significantly improve the quality and efficiency of seismic data processing, enhancing our understanding of hydrocarbon reservoirs and facilitating more accurate exploration and characterization of subsurface structures.

Keywords: Frequency domain · deep learning · seismic modelling · numerical dispersion · Fourier transform

1 Introduction

Simulating the wave field for a single seismic source takes several thousand core hours using conventional numerical modeling [15]. However, the acquisition system consists of thousands of seismic sources, resulting in high computational

Vadim Lisitsa and Kseniia Gadylshina developed frequency domain NDM-net approach and performed numerical experiments under the support of RSF grant no. 22-11-00004. Dmitry Vishnevsky performed seismic modeling using NKS-30T cluster of the Siberian Supercomputer Center under the support of basic research project FWZZ-2022-0022. Kirill Gadylshin optimized the NDM-net hyperparameters.

© The Author(s), under exclusive license to Springer Nature Switzerland AG 2023
O. Gervasi et al. (Eds.): ICCSA 2023 Workshops, LNCS 14106, pp. 31–44, 2023.
https://doi.org/10.1007/978-3-031-37111-0_3

costs. To address this issue, one possible approach is to reduce the dimension of the problem by decreasing the number of degrees of freedom or grid nodes. One way to achieve this is to increase the spatial grid step. Nonetheless, this leads to a numerical error, which frequently appears as numerical dispersion, especially when even-order approximations are used [1,10].

Deep learning has revolutionized the field of seismic processing by enabling automated, and more accurate interpretation of seismic data [17]. Seismic data is complex and multidimensional, and traditional processing methods have limitations in identifying subtle features and patterns in the data. Deep learning algorithms can automatically learn from large amounts of labeled data and identify patterns in seismic data that may be difficult for humans to detect [5]. This can lead to improved seismic imaging, better reservoir characterization, and more accurate predictions of subsurface properties. Deep learning also has the potential to reduce processing time and costs, making seismic exploration more efficient and cost-effective. Using machine learning methods to post-process seismic data seems promising, as suggested in the articles [6,13]. [4] describe an NDM-net artificial neural network that suppresses numerical dispersion. This deep neural network (DNN) is designed to suppress numerical dispersion in precalculated wave fields recorded at the free surface.

To generate realistic seismic data, wave fields must be computed for many source positions, typically on the order of 10^4. In such cases, seismograms for neighboring sources exhibit very slight differences [3]. A solution that closely approximates the actual one is employed as a representative dataset for training an artificial neural network to address this peculiarity of seismic modeling problems. This solution is obtained using a very fine grid, corresponding to a relatively small number of initial source positions. In a previous paper, [4], this approach was applied to two-dimensional models, and it was demonstrated that using seismograms from 10% of sources equidistantly distributed relative to each other as a training sample and post-processing them with a neural network, can significantly reduce the numerical error in data computed on a coarse grid. This approach reduces the time required to calculate the complete set of seismograms.

Treating seismic processing in the frequency domain involves analyzing seismic data in terms of its frequency content, providing numerous advantages over time-domain processing. By separating the different frequency components of the seismic signal, the frequency-domain method can help to identify subsurface features that may be difficult to detect in the time domain [16]. Additionally, frequency-domain methods can improve data quality by removing noise and correcting for amplitude and phase distortions caused by the seismic acquisition system [2,18]. Another benefit is that frequency-domain processing provides a more efficient way to extract information from seismic data, mainly when dealing with large data sets. Geoscientists can gain valuable insights into the subsurface by transforming seismic data into the frequency domain, leading to more accurate predictions about hydrocarbon reservoirs' location, size, and properties.

Frequency domain processing plays a critical role in modern seismic processing and can significantly improve the exploration and characterization of

hydrocarbon reservoirs by removing noise and distortions that may obscure essential features in the data. Moreover, much seismic processing is done in the frequency domain, with Full Waveform Inversion (FWI) being a prominent example [11]. FWI is closely related to seismic modeling and is often used in the time-frequency domain to better resolve subsurface structures and properties, leading to more accurate and detailed imaging results [14]. In this work, we present the application of NDM-net to seismic data in the frequency domain, highlighting the importance of using frequency-domain processing techniques in seismic exploration and imaging.

2 Theory and Method

2.1 Frequency Domain

We require fewer samples to work with seismic data in the frequency domain than in the time domain. To demonstrate this, we consider a typical synthetic reflection data shown in Fig. 1,A. It was modeled using an acoustic approximation with a Ricker source wavelet having a dominant frequency of 25Hz. The seismogram has a time step of 3ms and a length of 6s. The non-zero part of its Fast Fourier Transform (FFT) is presented in Fig. 1,B and C. The zoomed-in FFT for trace index 200 (vertical red line in Fig. 1,B) is plotted in Fig. 1,F and G. We can observe that only 512 frequency samples (red rectangle in Fig. 1,F and G) contain all the non-zero parts of the FFT signal.

To demonstrate this, we take this part's inverse FFT (IFFT) of the data (expanding all missing samples in the real and imaginary FFT parts using the zero value) and compare it with the original seismogram. The corresponding IFFT results and the difference with the original seismogram are presented in Fig. 1,C and D, respectively. One may observe that we don't lose information during these forward and inverse Fourier transforms. Similar property of FFT spectra of the solution of finite-difference problems is widely used in numerical simulations, including FFT-based data interpolation [9] and FFT-based preconditioners to solve Poisson equation [7].

In previous work [4], we could not process the full seismogram simultaneously due to GPU memory amount restrictions and had to split it in the time direction so that the processed part of the data had 512 time samples. Usually, in seismic modeling, we use a Ricker wavelet as a signal signature with a peak frequency of about $25 - 30$Hz, as the seismic data is band-limited, meaning that in the time-frequency domain, the primary energy of the signal is concentrated in a bounded band around the source peak frequency. In what follows, we will operate on the premise that synthetic seismic data is essentially band-limited.

2.2 NDM-Net in Frequency Domain

This study employs the NDM-net, which was introduced in [4]. This artificial neural network modifies the U-net, a fully convolutional neural network, as

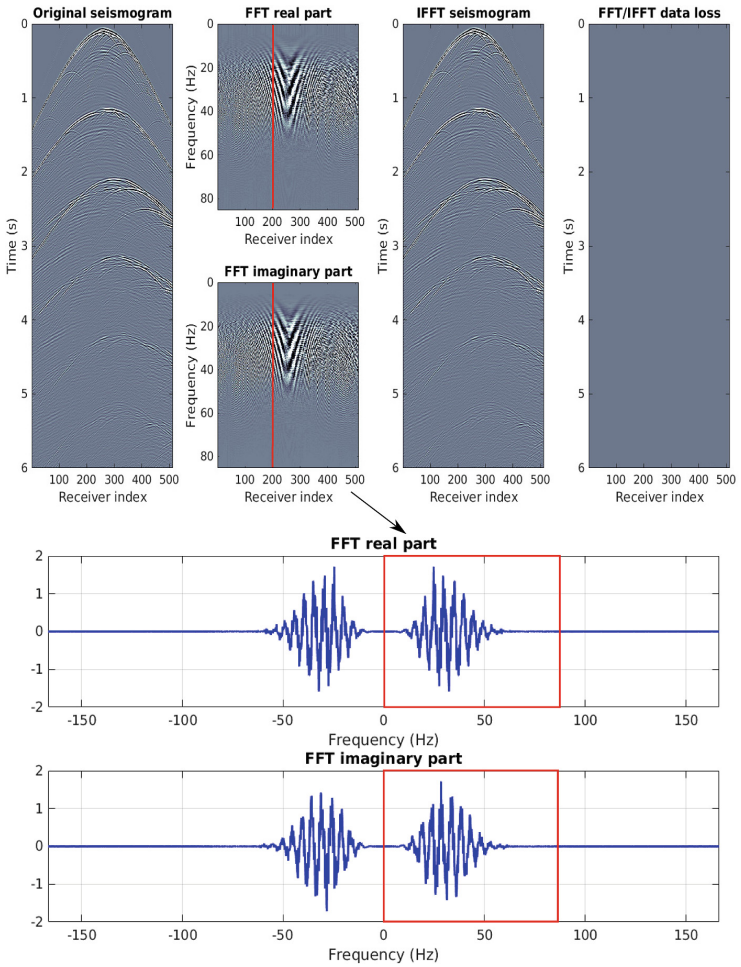

Fig. 1. The demonstration of time to frequency domain seismic data transform. The original seismogram (A), its Fourier transform (B), (C), and inverse Fourier transform (D). The difference between (A) and (D) is shown in plot(E) and demonstrates no loss of information during the time-frequency conversion. On the bottom, we present a particular trace in the frequency domain with index 200 (see vertical red line on (B), (C): real part (F) and imaginary part (G). The red rectangle demonstrates the part of the signal in the frequency domain used for data storing. (Color figure online)

described in [12]. The NDM-Net comprises 16 convolutional layers, eight upscaling layers, and eight concatenation layers, as illustrated in Fig. 2. The input and output tensors' dimensions are $512 \times 512 \times 2$. The activation function used for the first eight convolutional layers responsible for encoding or feature extraction is ReLU (linear rectification). For the last eight layers, representing the decoder part, the activation function used is LeakyReLu (linear rectification

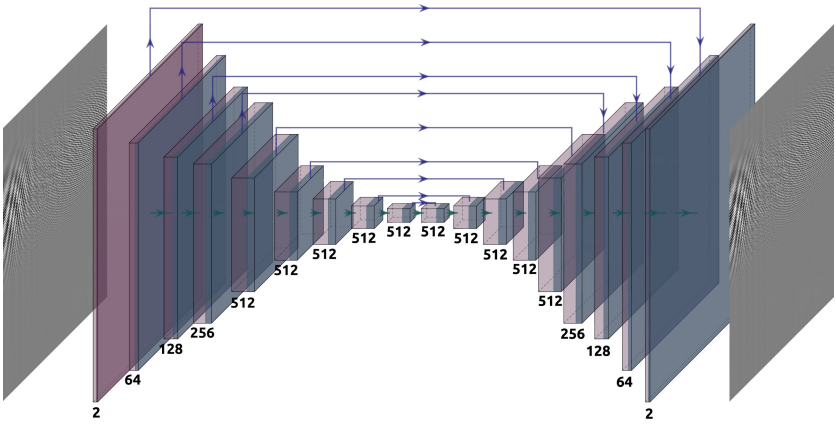

Fig. 2. FD NDM-net convolutional neural network architecture diagram. A convolutional neural network transforms frequency domain data calculated on a coarse grid (left) into data with suppressed numerical dispersion (right). The number of channels (depth) in the respective layers is indicated at the bottom under the layer blocks.

with a parameter), with a negative slope factor of 0.2. The PyTorch library is utilized for software implementation.

We use pre-calculated seismograms of a common source point on a fine grid to train the neural network, paired with their "distorted" versions modeled on a coarse grid. Seismograms at the input and output of NDM-net are recorded on the free surface. The seismogram is converted into a tensor of dimensions 512×512x2 to form the input data, where 512 corresponds to the number of frequencies, 512 corresponds to the number of receivers, and 2 corresponds to the real and imaginary parts of the FFT. The entire dataset is divided into a training set and a validation set in proportion 80% and 20%, respectively.

3 Numerical Experiment

All numerical experiments will be carried out using the realistic BP velocity model (Fig. 3). The left-hand side of the model is constructed using a geological cross-section that runs through the Western Gulf of Mexico. In the central part of the model, simplified representations of geological characteristics in the Eastern/Central Gulf of Mexico and off-shore Angola are depicted. The right-hand side of the model is a combination of representations of velocity challenges encountered in regions such as the Caspian Sea, North Sea, or Trinidad. This model is frequently used as a benchmark for prestack depth migration, especially reverse time migration.

The model extends 67.4 km horizontally and 11.9 km in vertical directions. The acquisition geometry consists of 2696 sources spaced equidistantly on the water surface with a step of 25m. For each source, we generate a synthetic seismogram recorded by 512 receivers, maximum source-receiver offset is 6.4

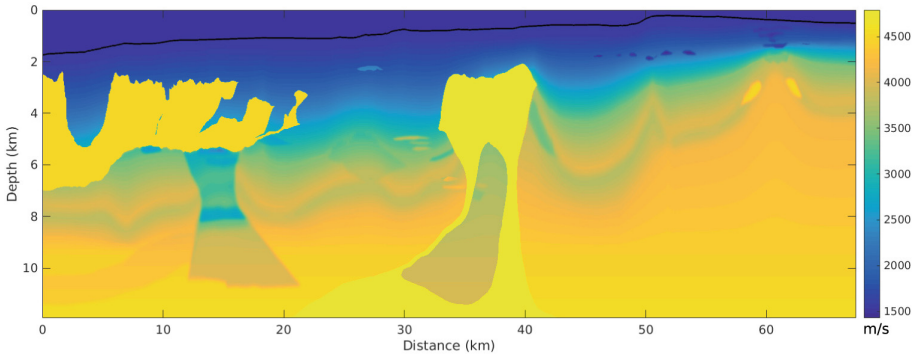

Fig. 3. BP velocity model. The black curve on the top of the model indicates the water bottom (first reflection surface).

km. The source signature is a Ricker wavelet with a peak frequency of 30Hz. We used a 4th-order finite-difference solver with absorbing boundary conditions at all model sides for modeling. We calculated the fine and coarse grid solutions on numerical grids with grid steps 3m and 6m, respectively.

3.1 Generating Training Dataset

As previously stated, we plan to handle seismic data in the frequency domain to process the complete seismogram at once without dividing it in the time domain. Using the characteristics of the BP velocity model (see the black curve in Fig. 3), we conduct an additional transformation in the time domain to align the primary water bottom reflection time across all source positions. As the velocity in the water remains constant in the model, any alterations in velocity begin beneath the water's bottom. This enables us to compute the double vertical time from the source to the corresponding water's bottom location and shift the synthetic seismogram accordingly.

Various approaches were studied in the time domain for performing the NDM-net training (references). In this work, we used 10% of the entire datasets for training, i.e., each 10th source position was used. After performing a time-shift transform, we perform FFT and obtain a training dataset in the frequency domain.

3.2 NDM-Net Training

The training was executed on a single GPU node equipped with dual RTX3090. The root mean square error was selected as the loss function, and we used the Adam optimizer ([8]) with an initial learning rate of 0.0002. During the training, we conducted 50 epochs, which took approximately 45 minutes. The corresponding training curves can be seen in Fig. 4. Subsequently, we employed the NDM-net weights acquired after the 47th epoch to conduct numerical dispersion

suppression on the entire dataset, which was calculated on a coarse grid. The prediction outcomes for a random seismogram from a testing dataset can be viewed in Fig. 5 and 6. Notably, a significant reduction in numerical dispersion is observed following NDM-net post-processing.

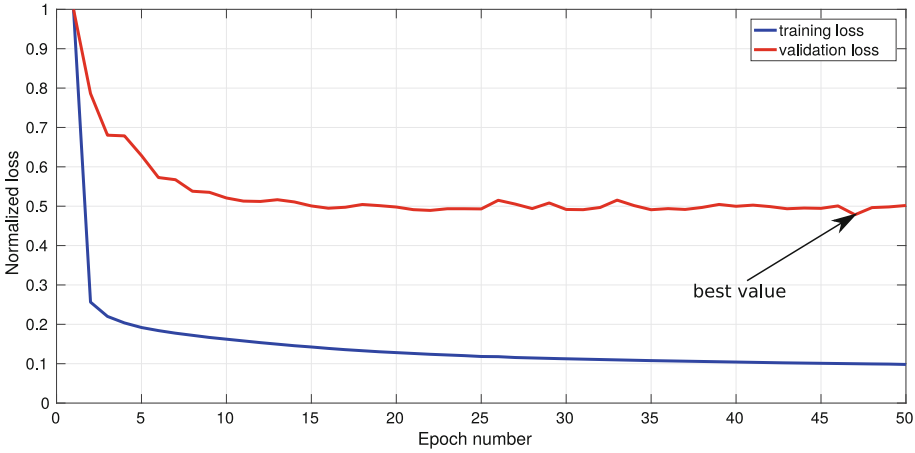

Fig. 4. The training (blue) and validation (red) losses are plotted in a normalized form. The black arrow indicates the best validation prediction results point (epoch number 47). (Color figure online)

3.3 Analyzing Numerical Results

In this study, we calculated the relative error between the fine and coarse grid solution or its NDM-net correction as a percentage using the following formula:

$$error_{relative}(A_i, B_i) = \frac{norm(A_i - B_i)}{norm(B_i)} \times 100\%, \tag{1}$$

here, A_i represents the coarse grid solution for a source with index i, B_i represents the corresponding fine grid solution, and $norm$ represents the Euclidean norm. The Euclidean norm is a commonly used metric to measure the error between two vectors. In this case, we used it to calculate the relative error between the solutions. The resulting error plot, which shows the level of numerical dispersion caused by rough finite difference approximation in dependence on the source position, is shown in Fig. 7 as a red plot. The plot indicates a significant level of numerical dispersion in the coarse grid solution, as evidenced by the high relative error.

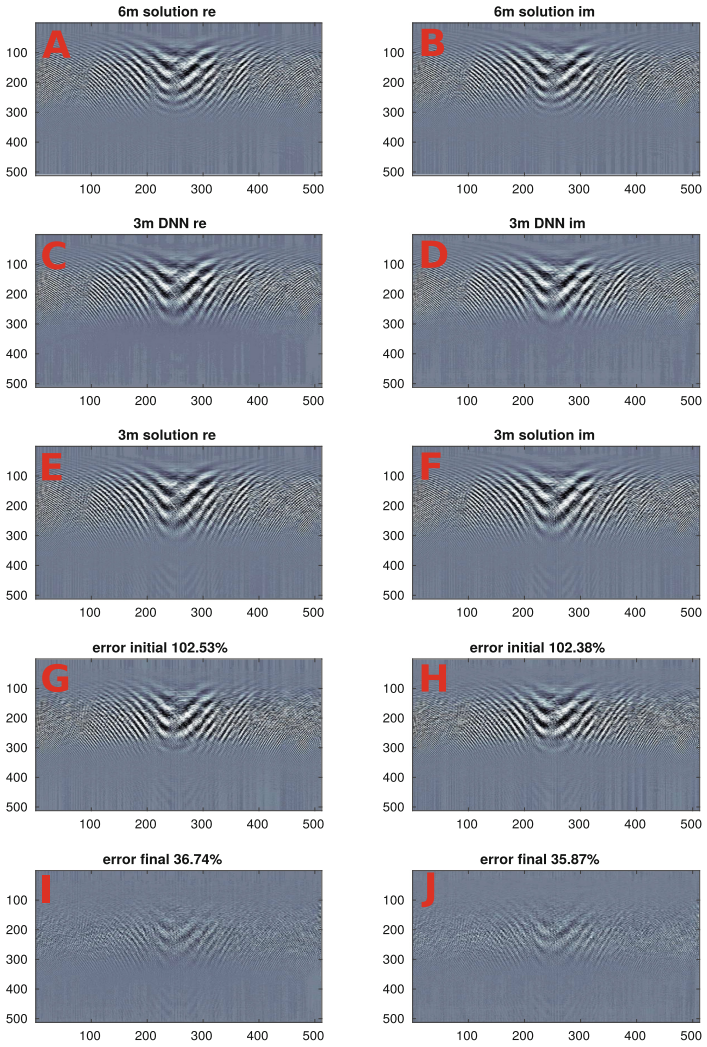

Fig. 5. The NDM-net prediction results for a source located at X=3.2 km. The left column is real parts, and the rights column is imaginary parts of the solution calculated on a coarse grid (A, B) and fine grid (E, F), NDM-net prediction results (C, D), the original dispersion (G, H) and the suppressed dispersion after NDM-net post-processing (I, J).

After performing the NDM-net post-processing and reducing the numerical dispersion in the data, we were able to construct the same relative error curve between the NDM-net predicted data and the fine grid solution. The NDM-net predicted error is plotted as a blue curve in Fig. 7, with a mean value of 31.49%

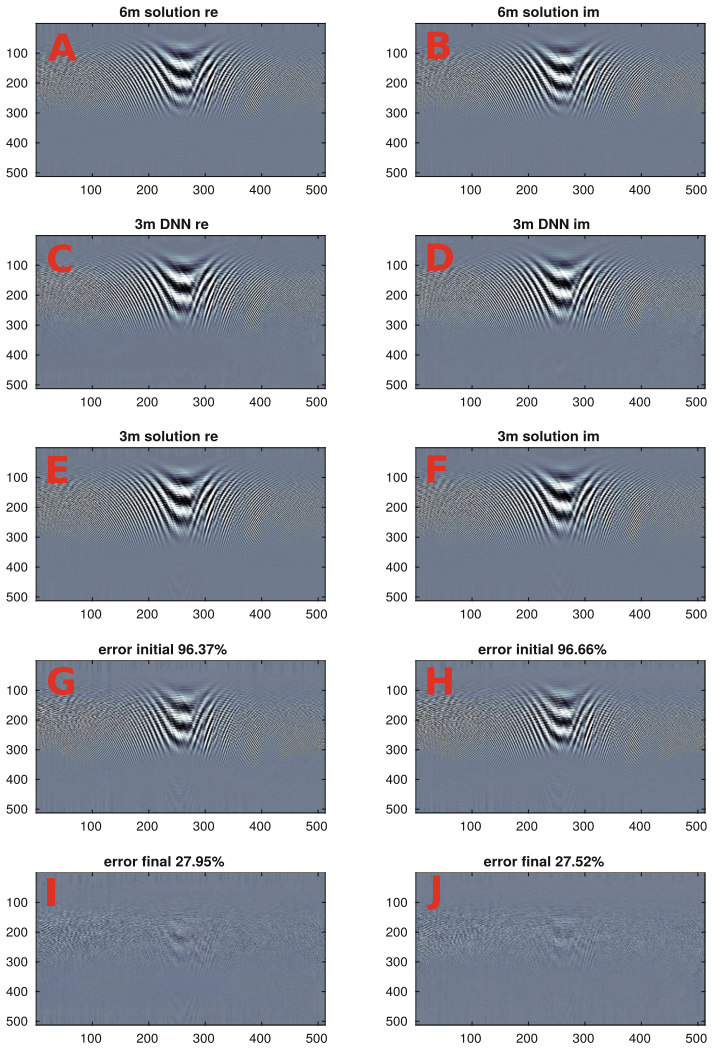

Fig. 6. The NDM-net prediction results for a source located at X=40.7 km. The left column is real parts, and the rights column is imaginary parts of the solution calculated on a coarse grid (A, B) and fine grid (E, F), NDM-net prediction results (C, D), the original dispersion (G, H) and the suppressed dispersion after NDM-net post-processing (I, J).

and a standard deviation of 7.13%. Therefore, we conclude that the level of numerical dispersion decreased three times after applying the NDM-net post-processing.

To better compare the coarse grid and the NDM-net predicted data, we selected two random source indexes from the testing dataset that the NDM-net did not use during training. Figs. 8 and 9 present the conversion of the frequency domain seismograms back to the time domain for these sources. Following Parseval's identity, which states that the Euclidean norm of the FFT seismogram is equal to its norm in the time domain, we observe a similar numerical dispersion level in the time domain.

We also provided trace-by-trace time domain/frequency domain comparisons for better visibility. These comparisons show that the NDM-net predicted and fine grid solutions have a good correlation in both the frequency and time domains, see Fig. 8F and Fig. 9F. The red plot represents the 6m solution, the black plot represents the 3m solution, and the blue plot represents the NDM-net prediction. We can observe a good correspondence between the seismic trace calculated on the fine grid and the NDM-net predictions, indicating the effectiveness of the NDM-net post-processing in reducing the level of numerical dispersion.

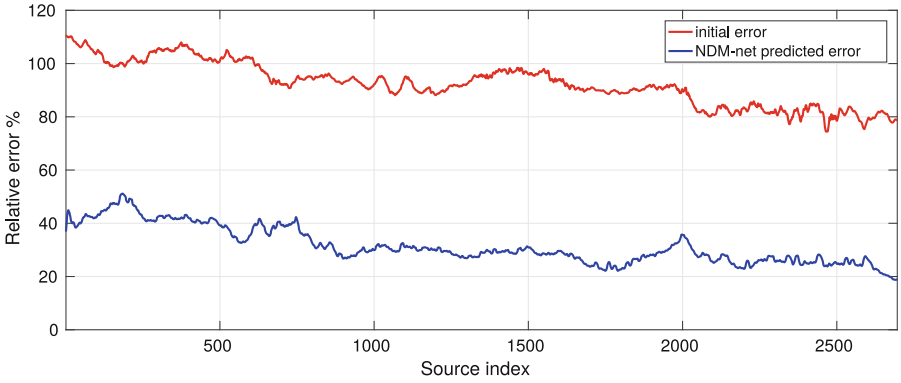

Fig. 7. The relative error between seismogram calculated on a coarse grid and fine grid solution (red plot), and the relative error between NDM-net post-processed seismogram and fine grid solution (blue plot). (Color figure online)

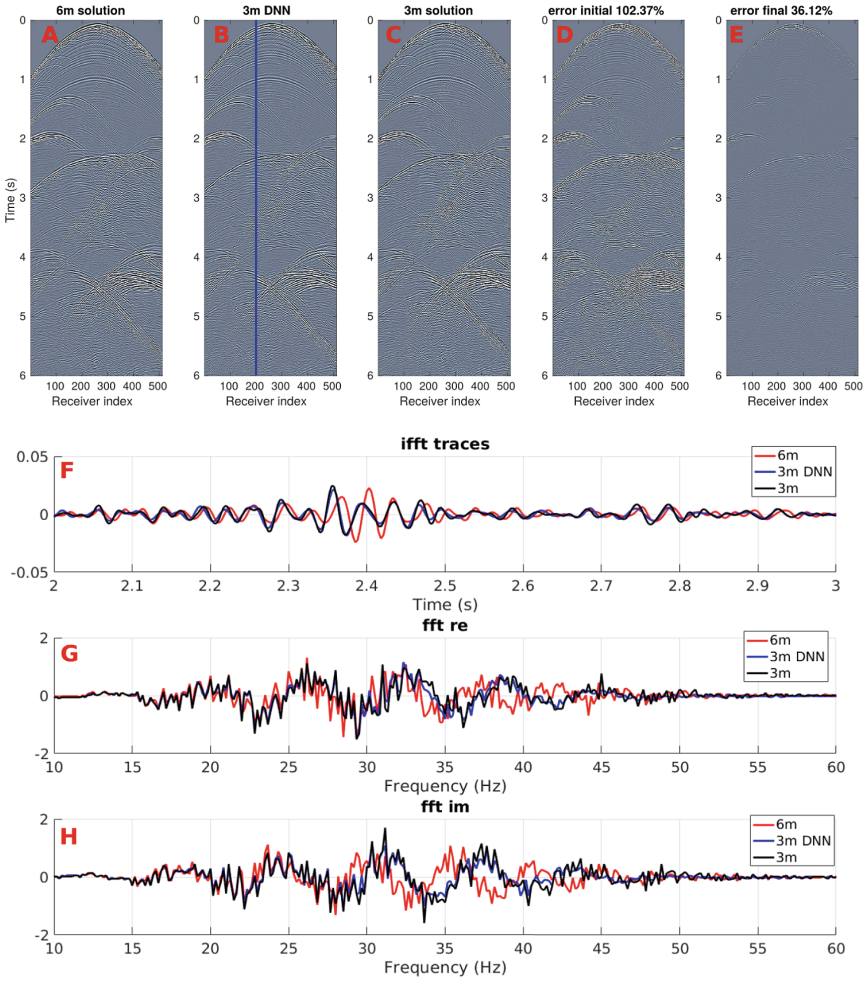

Fig. 8. The NDM-net prediction results for a source located at X=3.2 km converted back from frequency to the time domain. The seismogram modeled on coarse (A) and fine grid (C), the initial numerical dispersion (D) (difference between (C) and (A)), the NDM-net post-processed seismogram (B), and the suppressed numerical dispersion (E) (difference between (C) and (B)). The comparison of traces in the time (F) (trace index 200, see a blue line at (B)) and the frequency domain: real (G) and imaginary parts (H), respectively. Red plot - 6m solution, black plot - 3m solution, and blue plot - NDM-net prediction. (Color figure online)

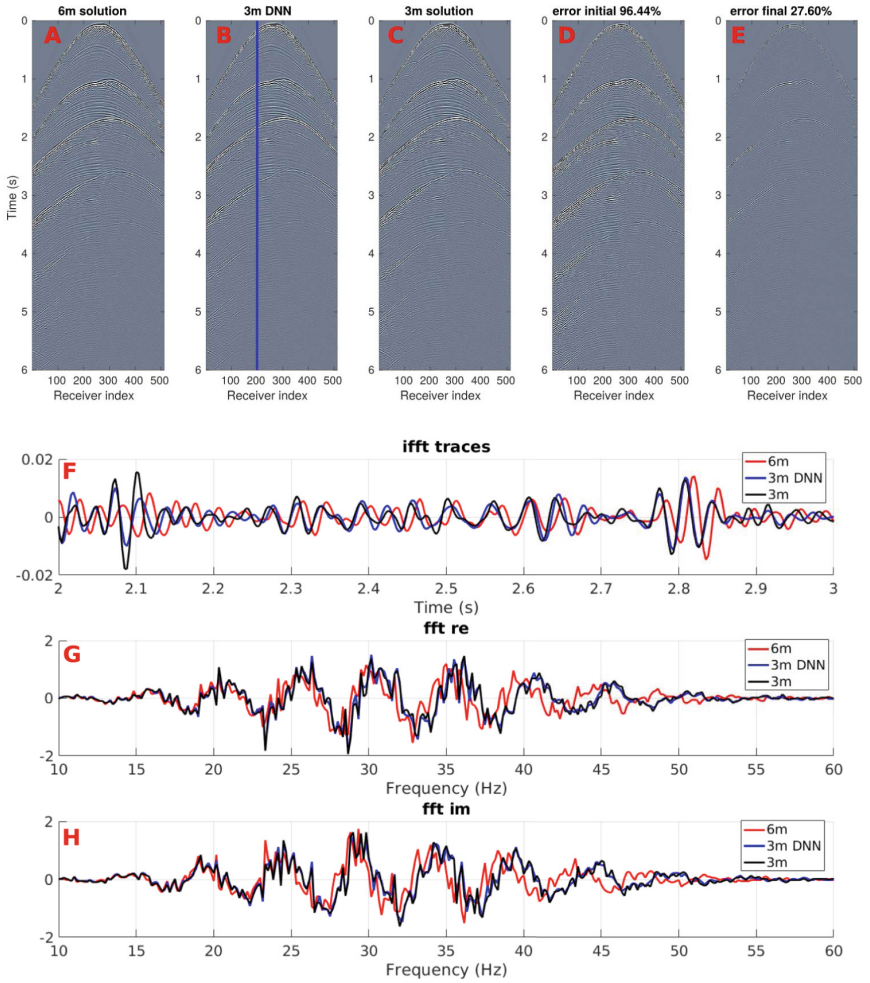

Fig. 9. The NDM-net prediction results for a source located at X=40.7 km converted back from frequency to the time domain. The seismogram modeled on coarse (A) and fine grid (C), the initial numerical dispersion (D) (difference between (C) and (A)), the NDM-net post-processed seismogram (B), and the suppressed numerical dispersion (E) (difference between (C) and (B)). The comparison of traces in the time (F) (trace index 200, see a blue line at (B)) and the frequency domain: real (G) and imaginary parts (H), respectively. Red plot - 6m solution, black plot - 3m solution, and blue plot - NDM-net prediction. (Color figure online)

4 Conclusions

In this study, we proposed using an NDM-net in the frequency domain to mitigate numerical dispersion in seismic data. Unlike time-domain processing, frequency-domain processing offers several advantages, including more efficient

extraction of information from large datasets, noise removal, and correction for amplitude and phase distortions. This approach can significantly enhance the exploration and characterization of hydrocarbon reservoirs, with Full Waveform Inversion (FWI) as a prominent example. We applied our proposed method to a realistic synthetic BP numerical example, which resulted in an average reduction of numerical dispersion by a factor of three and an order-of-magnitude increase in calculation performance. Our approach enabled us to process the entire seismogram simultaneously, in contrast to the time-domain NDM-net implementation. As a result, we can now apply this approach to 3D seismic modeling. Overall, using NDM-net in the frequency domain can significantly improve the quality and efficiency of seismic data processing. This approach could enhance our understanding of hydrocarbon reservoirs and facilitate more accurate exploration and characterization of subsurface structures.

References

1. Ainsworth, M.: Discrete dispersion relation for HP-version finite element approximation at high wave number. SIAM J. Numer. Anal. **42**(2), 553–575 (2004)
2. Elboth, T., Geoteam, F., Qaisrani, H.H., Hertweck, T.: De-noising seismic data in the time-frequency domain. In: SEG Expanded Abstracts, pp. 2622–2626 (2008)
3. Gadylshin, K., Lisitsa, V., Gadylshina, K., Vishnevsky, D.: Optimization of the training dataset for numerical dispersion mitigation neural network. In: Gervasi, O., Murgante, B., Misra, S., Rocha, A.M.A.C., Garau, C. (eds.) Computational Science and Its Applications - ICCSA 2022 Workshops. ICCSA 2022. Lecture Notes in Computer Science, vol. 13378, pp. 295–309. Springer, Cham (2022). https://doi.org/10.1007/978-3-031-10562-3_22
4. Gadylshin, K., Vishnevsky, D., Gadylshina, K., Lisitsa, V.: Numerical dispersion mitigation neural network for seismic modeling. Geophysics **87**(3), T237–T249 (2022)
5. Goodfellow, I.J., Bengio, Y., Courville, A.: Deep Learning. MIT Press, Cambridge (2016). http://www.deeplearningbook.org
6. Kaur, H., Fomel, S., Pham, N.: Overcoming numerical dispersion of finite-difference wave extrapolation using deep learning. In: SEG Technical Program Expanded Abstracts, pp. 2318–2322 (2019).https://doi.org/10.1190/segam2019-3207486.1
7. Khachkova, T., Lisitsa, V., Reshetova, G., Tcheverda, V.: GPU-based algorithm for evaluating the electrical resistivity of digital rocks. Comput. Math. Appl. **82**, 200–211 (2021)
8. Kingma, D., Ba, J.: Adam: a method for stochastic optimization. In: International Conference on Learning Representations (2014)
9. Kostin, V., Lisitsa, V., Reshetova, G., Tcheverda, V.: Local time-space mesh refinement for simulation of elastic wave propagation in multi-scale media. J. Comput. Phys. **281**, 669–689 (2015)
10. Lisitsa, V.: Dispersion analysis of discontinuous Galerkin method on triangular mesh for elastic wave equation. Appl. Math. Model. **40**, 5077–5095 (2016). https://doi.org/10.1016/j.apm.2015.12.039
11. Pratt, R.G., Shin, C., Hick, G.J.: Gauss-Newton and full Newton methods in frequency-space seismic waveform inversion. Geophys. J. Int. **133**(2), 341–362 (1998)

12. Ronneberger, O., Fischer, P., Brox, T.: U-Net: convolutional networks for biomedical image segmentation. In: Navab, N., Hornegger, J., Wells, W.M., Frangi, A.F. (eds.) MICCAI 2015. LNCS, vol. 9351, pp. 234–241. Springer, Cham (2015). https://doi.org/10.1007/978-3-319-24574-4_28
13. Siahkoohi, A., Louboutin, M., Herrmann, F.J.: The importance of transfer learning in seismic modeling and imaging. Geophysics **84**, A47–A52 (2019). https://doi.org/10.1190/geo2019-0056.1
14. Tcheverda, V., Gadylshin, K.: Elastic full-waveform inversion using migration-based depth reflector representation in the data domain. Geosciences **11**(2) (2021)
15. Virieux, J., Calandra, H., Plessix, R.E.: A review of the spectral, pseudo-spectral, finite-difference and finite-element modelling techniques for geophysical imaging. Geophys. Prospect. **59**(5), 794–813 (2011). https://doi.org/10.1111/j.1365-2478.2011.00967.x
16. Yilmaz, Ö., Doherty, S.: Seismic Data Analysis: Processing, Inversion, and Interpretation of Seismic Data. In: Crisp Fifty-Minute Books, Society of Exploration Geophysicists, no. 10, vol. 1 (2001)
17. Yu, S., Ma, J.: Deep learning for geophysics: current and future trends. Rev. Geophys. **59**(3), e2021RG000742 (2021)
18. Zhao, Y., Liu, Y., Li, X., Jiang, N.: Time-frequency domain snr estimation and its application in seismic data processing. J. Appl. Geophys. **107**, 25–35 (2014)